
Article:
Andrews, T, Smith, CJ orcid.org/0000-0003-0599-4633, Myhre, G et al. (3 more authors) (2021) Effective radiative forcing in a GCM with fixed surface temperatures. Journal of Geophysical Research: Atmospheres, 126 (4). ISSN 2169-897X

https://doi.org/10.1029/2020jd033880

Effective radiative forcing in a GCM with fixed surface temperatures

Timothy Andrews[1,*], Christopher J. Smith[2,3], Gunnar Myhre[4], Piers M. Forster[2], Robin Chadwick[1,5] and Duncan Ackerley[1]

[1]Met Office Hadley Centre, Exeter, UK.

[2] Priestley International Centre for Climate, University of Leeds, UK.

[3]International Institute for Applied Systems Analysis (IIASA), Laxenburg, Austria.

[4]Center for International Climate and Environmental Research, Oslo, Norway.

[5]Global Systems Institute, University of Exeter, Exeter, UK.

Submitted to *Journal of Geophysical Research: Atmospheres*

10th September 2020

Revised: 19h November 2020

Key Points:

- $4xCO_2$ ERF is ~1 Wm^{-2} less in a typical GCM ERF experiment with fixed-SST compared to an ERF experiment with fixed SST and land temperatures.
- This is due to the influence of land warming on temperature, lapse-rate, water-vapour, surface albedo and clouds in the fixed-SST experiment.
- Previous methods used to account for land warming in fixed-SST ERF experiments are evaluated.

*Corresponding author address:

Met Office Hadley Centre

FitzRoy Road

Exeter

EX1 3PB, UK.

Email: timothy.andrews@metoffice.gov.uk

Abstract

Effective radiative forcing (ERF) is evaluated in the ACCESS1.0 General Circulation Model (GCM) with fixed land and sea-surface-temperatures as well as sea-ice. The 4xCO_2 ERF is 8.0 Wm^{-2}. In contrast, a typical ERF experiment with only fixed sea-surface-temperatures (SST) and sea-ice gives rise to an ERF of only 7.0 Wm^{-2}. This difference arises due to the influence of land warming in the commonly used fixed-SST ERF experimental design, which results in: (i) increased emission of longwave radiation to space from the land surface (-0.45 Wm^{-2}) and troposphere (-0.90 Wm^{-2}), (ii) reduced land snow-cover and albedo (+0.17 Wm^{-2}), (iii) increased water-vapour (+0.49 Wm^{-2}), and (iv) a cloud adjustment (-0.26 Wm^{-2}) due to reduced stability and cloudiness over land (positive ERF) counteracted by increased lower tropospheric stability and marine cloudiness over oceans (negative ERF) . The sum of these radiative adjustments to land warming is to reduce the 4xCO_2 ERF in fixed-SST experiments by ~1.0 Wm^{-2}. CO_2 stomatal effects are quantified and found to contribute just over half of the land warming effect and adjustments in the fixed-SST ERF experimental design in this model. The basic physical mechanisms in response to land warming are confirmed in a solar ERF experiment. We test various methods that have been proposed to account for land warming in fixed-SST ERFs against our GCM results and discuss their strengths and weaknesses.

Plain language summary

Radiative forcing measures the energy imbalance caused by anthropogenic activities (such as emissions of CO_2, other greenhouse gases or aerosols) or natural events (such as volcanic eruptions). There are various definitions of radiative forcing, with the most commonly used being the 'effective radiative forcing' which measures the energy imbalance after allowing for atmospheric temperatures, water vapour and clouds to adjust to the forcing agent, while keeping surface conditions (specifically temperature) unchanged. However in complex climate models it is difficult to prescribe land temperatures, so in practice ERF estimates are generally contaminated by the radiative effect of land temperature change and responses to it. Here we quantify this effect for the first time, finding that for 4xCO_2, the ERF is reduced by ~1.0 Wm^{-2} (~14%) in a typical climate model ERF experiment due to land warming and its impact on temperatures, water-vapour, clouds and surface albedo.

1. Introduction

Radiative forcings have long been used to compare and rank the drivers of past and future climate change (e.g. Shine and Forster, 1999; Shine et al., 2003; Hansen et al., 2005). Various definitions of radiative forcing have emerged over the years (Ramaswamy et al. 2018), each with their own strengths and weaknesses (Hansen et al. 2005). 'Effective radiative forcing' (ERF) is now the most widely adopted definition of radiative forcing (Myhre et al., 2013; Boucher et al. 2013; Sherwood et al., 2015; Forster et al., 2016; Ramaswamy et al. 2018) since it has been found to be the best predictor of the resulting climate response (Shine et al., 2003; Hansen et al., 2005; Richardson et al., 2019), measured by global-mean surface-air-temperature change, Δ*T*.

Myhre et al. (2013) defined ERF to be the "*change in the net TOA downward radiative flux after allowing for atmospheric temperatures, water vapour and clouds to adjust, but with surface temperature or a portion of surface conditions unchanged*". Hence ERF not only includes the 'instantaneous radiative forcing' (IRF) (i.e. the instantaneous change in radiative flux caused by the introduction of a forcing agent) but also any other responses (often called 'adjustments') to forcing that are not mediated by surface temperature change (Boucher et al. 2013; Sherwood et al., 2015; Ramaswamy et al., 2018).

A self-consistent forcing-feedback framework requires forcing adjustments to be separated from feedback by identifying radiative responses that are not mediated by Δ*T* (Shine et al., 2003; Hansen et al., 2005; Sherwood et al., 2015; 2020). In practice however, this separation is inconsistent with the way the community generally calculates ERF in General Circulation Models (GCMs), which use the recommended method of only fixing sea-surface-temperatures and sea-ice fraction (e.g. Myhre et al., 2013; Forster et al., 2016; Pincus et al., 2016) with land temperatures being free to respond[1]. This is partly a pragmatic recommendation since prescribing land surface conditions in a GCM – while possible – presents a technical challenge (see Hansen et al, 2005; Ackerley and Dommenget, 2016; Ackerley et al., 2018). Indeed Hansen et al. (2005) were unable to find a satisfactory method in their own model, but noted this may be due to their model-specific formulations. Only Shine et al. (2003) have provided ERF estimates with fixed surface temperatures everywhere, but this was only achievable in a GCM of 'intermediate complexity' which they defined as having '*physical parameterisations (radiation, clouds, surface flux) … typical of what would have been state of the art in the 1980s*'.

Hence in typical GCM fixed-SST ERF calculations land temperatures are free to respond to the forcing and so some Δ*T*-mediated responses may arise that might be better considered a feedback and so contaminate the ERF calculation. Hansen et al. (2005) proposed a correction to the fixed-SST method to account for this by assuming the radiative response to Δ*T* arising from land temperature change could be calculated from the model's long-term feedback parameter. Smith, Kramer and Myhre et al. (2020) provide an alternative approach where the radiative effect of the land surface temperature change is calculated using radiative kernels and subtracted from the ERF. Tang et al. (2019) also use a kernel approach but additionally calculate other radiative responses that can reasonably be assumed to be associated with the land surface temperature change, such as changes in surface albedo and a component of tropospheric temperature (assumed to be vertically uniform and equal to that of the surface) and associated water-vapour change. None of these methods have

[1] An alternative method for estimating ERF is the Gregory-type regression method (Gregory et al., 2004), but here our focus is on the fixed-SST GCM experiments to determine ERF. Note that the two methods are in principle different (see Summary and Discussion, Section 5).

been tested against a GCM calculation of ERF with fixed surface temperatures over land as well as SST, something we aim to do here.

Here we use the modelling framework of Ackerley and Dommenget (2016) and Ackerley et al. (2018) for prescribing land temperatures in the Australian Community Climate and Earth System Simulator (ACCESS) GCM to calculate ERF in both a fixed-SST and fixed surface temperatures (SST and land) (T_s) experimental design in a complex GCM for the first time. This allows us to isolate and quantify the radiative effect and adjustments associated with land temperature change in the commonly used fixed-SST ERF experimental design, provide a physical description of the relevant processes and test the various methods that have been proposed to account for land warming effects in ERFs. Our principle focus is on a forcing from a quadrupling of CO_2, but we also isolate a CO_2 stomatal-conductance effect by analysing experiments with different biogeochemical couplings. We further check the robustness of the basic physical processes we describe by a comparison to an ERF from a change in the solar constant. The experimental design therefore allows the effects of land warming, reduced atmospheric radiative cooling and plant transpiration in response to increased CO_2 to be separated. Chadwick et al. (2019) provide a description of the circulation and precipitation changes in these experiments, while Kamae et al. (2019) analysed the seasonality of the marine low cloud adjustments. Here our focus is on the ERF and adjustments in these experiments.

2. Method

2.1 GCM Experiments

We use the Prescribed Land AMIP (PLAMIP) v1.0 dataset as described in Ackerley et al. (2018). The GCM used in PLAMIP is an atmosphere-only configuration of ACCESS1.0. ACCESS1.0 is a CMIP5 generation model and described in detail in Bi et al., (2013). However the version of ACCESS1.0 used in PLAMIP has a horizontal grid spacing of 3.75° (longitude) × 2.5° (latitude) and 38 vertical levels, which is slightly lower in horizontal resolution than the ACCESS1.0 submissions to CMIP5. ACCESS1.0 shares the same atmospheric physics as that of the Hadley Centre Global Environmental Model version 2 (HadGEM2) (Martin et al., 2011) and the same land surface scheme, namely the Met Office Surface Exchange Scheme (MOSES) version 2.2 (Essery et al., 2003). MOSES is a somewhat simpler scheme than more recent developments used in the latest (e.g. CMIP6) generation of models, such as its successor in either the HadGEM family of models (which now use the Joint UK Land Environment Simulator, JULES, Best et al., 2011) or the ACCESS family of models (which now use The Community Atmosphere Biosphere Land Exchange, CABLE, model, e.g. Kowalczyk et al., 2013). A dynamic vegetation scheme is not included, so vegetation cover is fixed. Note that the similarity of ACCESS1.0 to the HadGEM family of models is useful for assumptions made in Section 2.2.

The control simulation is an AMIP type simulation (e.g. Gates et al., 1999), i.e. the AGCM is prescribed with seasonally varying monthly-mean observed SSTs and sea-ice fraction, land temperatures being free to evolve. Forcing levels, e.g. greenhouse gas levels and aerosol emissions, are kept constant as described in Ackerley et al. (2018). The background climatology is to some extent immaterial for ERF simulations (Forster et al., 2016) but is described and evaluated in detail in Ackerley et al. (2018) and is found to compare well against observations and is comparable with other CMIP5 generation models (in terms of 1.5 m temperature, precipitation and mean sea level pressure biases). From this control simulation, three fixed-SST ERF simulations are performed: (i) CO_2 is quadrupled from 346ppm to 1384 ppm ($4xCO_2$), (ii) CO_2 is quadrupled only in the radiation scheme, the vegetation scheme continues to 'see' control levels of CO_2 ($4xCO_2$-rad), and (iii) an

increase in the solar constant by ~3.3% from 1365 Wm^{-2} to 1410.7 W m^{-2} (+Solar). 4xCO_2-rad follows the analogous experimental design of Doutriaux-Boucher et al. (2009) who showed that plant physiological processes – specifically a reduced stomatal opening in the plant's leaves in response to elevated CO_2 (e.g. Field et al., 1995) – can have a large impact on CO_2 ERF. This occurs via reduced evapotranspiration which influences moisture availability, boundary layer humidity and cloud cover, temperature and precipitation, amongst other things (e.g., Andrews et al., 2011; Arellano et al., 2011; Andrews and Ringer, 2014). The comparison of 4xCO_2 to 4xCO_2-rad allows us to quantify this effect, and since such CO_2 physiological processes will not occur under non-CO_2 forcings, inhibiting this process (4xCO_2-rad) allows a clean comparison of physical processes with those in the +Solar ERF experiment.

To generate ERF simulations with fixed land temperatures as well SSTs, the surface temperature, soil moisture and deep soil temperatures from the AMIP control simulation (described above) is saved and then used in re-runs of both the control and perturbation ERF simulations with those fields prescribed. Full details of the experimental setup are given in Ackerley et al. (2018) and further details on developing the prescribed land method are described by Ackerley and Dommenget (2016) and so a brief description of the experiments is given here. Three-hourly surface temperature, soil moisture and deep soil temperature are taken from the control simulation (i.e. free running land conditions) described above. The three-hourly fields are read in by the prescribed land model where they are interpolated in time to allow the fields to be updated hourly (details of the physical changes are described in Ackerley et al., 2018). Timestep frequency data is not used because of practical limitations of reading in such large datasets (Ackerley et al. 2018). However, Ackerley and Dommenget (2016) showed that a simulation using timestep data was almost indistinguishable from another using interpolated three-hourly data. By using three-hourly surface temperature, soil moisture and deep soil temperature, the model will retain a diurnal cycle in each of those fields as well as physical consistency between them (i.e. each prescribed field is dependent on the other and so it is important to prescribe all three). The prescribed land simulations therefore closely mimic the intended (freely evolving land) control experiment for the entirety of their simulation (discussed in detail in Ackerley et al., 2018).

An important limitation is that the method cannot prescribe surface temperatures over both the permanent ice sheets (Greenland and Antarctica) and over sea-ice (Ackerley and Dommenget, 2016; Ackerley et al. 2018). While this has negligible impact on the climatology of these simulations (Ackerley et al., 2018) we do find that that global-mean surface temperature change, ΔT_s, is close to – but not precisely – zero in our ERF experiments, and this results in a small but non-zero surface temperature and Planck adjustment in our results (see Section 3). While imperfect we accept this as a technical limitation of the experimental design.

Our analysis period covers a common 29 years of model simulation (Jan 1980 through to Dec 2008 in model time) except for the 4xCO_2-rad simulations which we limit to 20 years (Jan 1980 to Dec 1999) because an issue with the remaining 9 years (Jan 2000 to Dec 2008) of the prescribed land 4xCO_2-rad simulation was discovered during analysis. There is now clear instruction not to use those years on the PLAMIP data site[2]. The shorter time-period over which the ERF is calculated reduces the signal to noise ratio in this simulation but does not bias the result relative to the longer simulations, assuming there is no dependence of the ERF on the underlying background state which is varying (Forster et al. 2016). Indeed, if we restrict our 4xCO_2 fixed-SST ERF data to just 20 years we confirm that the same global-time-mean ERF (7.03 Wm^{-2}) is returned as when using the full 29 years of data. Hence we use

[2] https://researchdata.edu.au/prescribed-land-amip-v10-amip/1330579

the full timeseries of data where possible to reduce noise, rather than restricting all analysis to a common 20 year period.

To summarise, we have a set of 4xCO_2, 4xCO_2-rad and Solar ERF experiments with fixed-SSTs and fixed-surface temperatures (referred to as fixed-T_s). The climatology of the simulations and validation of the methodology is extensively documented and analysed in Ackerley et al. (2018). This includes additional experiments to validate the linearity of assuming the land warming effect as the difference between these sets of experiments, which is what we do here.

2.2 ERF, radiative kernels and adjustments

The ERF used here is does not have a strict definition but is taken to include responses beyond the IRF and is calculated simply as the change in TOA radiative flux in the perturbation experiment relative to its control (e.g. Forster et al., 2016), in this case averaged over the 29 years of simulation (20 years in the 4xCO_2-rad case). We separate the ERF into its IRF and adjustment processes following the radiative kernel technique as described, for example, in Smith et al. (2018). Briefly, we write the ERF as

$$\text{ERF} = \text{IRF} + A_{Planck_{surf}} + A_{Planck_{trop}} + A_{LR} + A_{strat} + A_q + A_\alpha + A_c + \epsilon,$$

where A_x is the adjustment x in forcing due to: (1) surface temperature change (i.e. the surface Planck response, $Planck_{surf}$), (2) a vertically uniform temperature change (equal to that of the surface temperature change) throughout the troposphere (i.e. the tropospheric Planck response, $Planck_{trop}$), (3) a change in the tropospheric lapse-rate (LR) (i.e. the deviation from vertically uniform temperature change), (4) stratospheric temperature ($strat$) change, (5) water-vapour (q) change, (6) surface albedo (α) change, (7) changes in cloudiness (c), and finally ϵ is a residual that accounts for nonlinearities and kernel errors. This separation into adjustment terms is analogous to how the climate feedback community isolate various feedback processes (e.g. Bony et al., 2006; Soden et al. 2008). Note the feedback literature typically sum the $Planck_{surf}$ and $Planck_{trop}$ terms into a single 'Planck response', but here we will find it to be useful to have separated the surface and tropospheric components. The Planck response is often considered to be a horizontally and vertically uniform temperature response, but in GCM calculations it is typically estimated from the surface temperature change applied to each level (Bony et al., 2006) as we have done here. Hence while vertically uniform, it is not necessarily horizontally uniform, and this will certainly be the case in our experiments where land temperatures are free to evolve but SSTs are fixed. An alternative approach would be to simply sum the tropospheric Planck and lapse-rate terms (i.e. $A_{Planck_{trop}} + A_{LR}$) into a single tropospheric temperature response as per Smith et al. (2018; 2020), but we find the isolation of a lapse-rate term useful for linking to stability changes and it is required for the application of the Tang et al. (2019) method in Section 4.3.

We separate the stratosphere and troposphere using a tropopause that varies linearly from 100 hPa at the equator to 300 hPa at the poles following Soden et al. (2008). Each adjustment A_x is determined by multiplying the change in variable ($\Delta x = x_{\text{pert}} - x_{\text{cntl}}$) in the ERF experiment by the relevant radiative kernel K_x that describes the TOA radiative flux change for a unit change in variable x. We use radiative kernels derived from the HadGEM3-GA7.1 model (Smith, Kramer and Sima et al. 2020) which has a similar radiation scheme to ACCESS1.0. All calculations are preformed on monthly-mean data.

Cloud adjustments, A_c, are calculated by correcting the change in 'cloud radiative effect' (CRE) (defined as the difference between all-sky and clear-sky radiative flux changes, i.e. ERF - ERF^{clr}) for 'cloud masking effects' (see Soden et al., 2008). Following Smith et al. (2018) we write,

$$A_c = (ERF - ERF^{clr}) - (IRF - IRF^{clr}) - \sum_x (A_x - A_x^{clr}),$$

where superscript 'clr' refers to clear-sky radiative fluxes and the A_x^{clr} terms are calculated as above but using corresponding clear-sky radiative kernels. $4xCO_2$ IRF and IRF^{clr} are taken from the closely related HadGEM2 model, calculated from instantaneous double calls to the radiation scheme in the CMIP5 amip-$4xCO_2$ experiment (Taylor et al., 2012). We also assume these HadGEM2 IRFs in the surface albedo calculation (see below). Assuming the IRF from a model closely related to ACCESS1.0 may be imperfect, but no more so than the application of the radiative kernel method in general, which is only ever an approximation of the radiative transfer of a model. Moreover IRF is not our primary focus here and is identical in fixed-SST and fixed-T_s experiments by design. The solar IRF is calculated from the change in insolation, the model's planetary albedo (μ) and geometry, so that IRF – IRF^{clr} = $\Delta SW_{\downarrow}(\mu^{clr}-\mu)$ where $SW_{\downarrow}$ is the incoming TOA SW radiation and μ^{clr} and μ are the control clear-sky and all-sky TOA planetary albedo.

An issue with the PLAMIP dataset is that the surface fluxes required to directly calculate the change in surface albedo change, $\Delta\alpha$, do not exist. A similar issue was encountered by Sanderson et al. (2010) when applying radiative kernels to the climate*prediction*.net dataset. We use an expansion of their solution here. We calculate the clear-sky albedo adjustment A_α^{clr} by assuming it to be the residual between the SW clear-sky ERF, ΔSW^{clr}, and the effects of CO_2 IRF and water-vapour change on the SW clear-sky budget (since these are the only other dominant terms that will affect the SW clear-sky budget). That is,

$$A_\alpha^{clr} = \Delta SW^{clr} - SW\_IRF^{clr} - SW\_K_q^{clr}\Delta q.$$

Since $A_\alpha^{clr} = K_\alpha^{clr}\,\Delta\alpha$, we can then calculate $\Delta\alpha = A_\alpha^{clr} / K_\alpha^{clr}$, which can be used with the all-sky kernel as normal to calculate A_α. The surface albedo change ought to be zero over the ice-free oceans in these experiments (Smith, Kramer and Myhre et al., 2020), which we enforce by masking out ocean points between 58.75°S to 58.75°N.

A final issue is that the dataset does not contain a Heaviside function which is needed to weight 3D fields to account for sub-orographic data. This would lead to erroneous data passing into our calculations if not accounted for. To account for this, we check each grid point's monthly-mean pressure level (p) against the model's surface pressure (p_s): if $p > p_s$ (i.e. sub-orographic) we mask out the data. To account for variations in pressure levels below our monthly-mean calculations (i.e. a grid box may have been sub-orographic for part of a month), we conservatively apply an extra 2000Pa to the model's pressure level. This ensures all data in our calculations are valid, though at the expense of potentially masking out some valid data.

3. Results

3.1. Surface temperature change and ERF

Figure 1a,b shows the surface temperature change in the two ERF experimental designs under $4xCO_2$ alongside the corresponding ERFs (Figure 1d,e). As desired and constructed, the surface temperature change in the $4xCO_2$ ERF experiment with fixed-SST (Figure 1a) arises almost entirely over land

(temperatures over sea-ice varying a small amount). When land surface properties are additionally prescribed (the fixed-T_s experiment), the surface temperature change is near zero almost everywhere (Figure 1b), noting the limitation that temperatures are not prescribed over ice-sheets or sea-ice. Global-mean surface temperature change, ΔT_s, is 0.51 K in the fixed-SST experiment but only 0.04 K in the fixed-T_s experiment (Table 1). The global-mean surface-air-temperature changes, ΔT, are 0.56 K and 0.13 K respectively (Table 1). That $\Delta T > \Delta T_s$ is because, as described in Ackerley et al. (2018), the calculation of surface-air-temperature is an interpolation between the surface temperature and that of the lowest model level, hence changes in surface-air-temperature can arise from changes in the model's lowest level as a legitimate response to CO_2 increase even if surface temperatures are unchanged.

Figure 1d,e shows the geographical distribution of the 4xCO_2 ERF under the two experimental designs, alongside their difference (Figure 1f) which we interpret as the radiative effect of land warming in the fixed-SST design. Under fixed-SST the global-mean 4xCO_2 ERF is 7.0 Wm^{-2} but this increases to 8.0 Wm^{-2} under fixed-T_s. Hence the radiative effect of land warming (and associated forcing adjustments described in the next Section) reduces the 4xCO_2 ERF by ~1.0 Wm^{-2} in this model.

3.2. Adjustment processes

Table 1 presents the global-mean ERF and radiative adjustments for all forcing experiments (e.g. 4xCO_2, 4xCO_2-rad and +Solar) under both fixed-SST and fixed-T_s ERF experimental designs, as well as their difference, which we interpret as the ERF and radiative adjustments associated with the land surface temperature change in the fixed-SST design. For ease of comparison, the 4xCO_2 fixed-SST and fixed-T_s results are depicted in Figure 2.

The surface temperature adjustment (i.e. $A_{Planck_{surf}}$) is – as constructed – near zero in the fixed-T_s design for all forcings (Table 1), but large in the fixed-SST experiment when land temperatures are allowed to warm (Table 1 and Figure 2b for 4xCO_2). Similarly, the surface albedo adjustment (A_α) is large in the fixed-SST design but near zero when land temperatures are fixed, as expected since land snow cover change is driven by surface warming (Table 1). The geographical distributions of the 4xCO_2 radiative adjustments in both experimental designs and their difference (the land effect) are shown in Figure 3 (see Supporting Information Figures S1 and S2 for the 4xCO_2-rad and +Solar experiments). Both the surface temperature and surface albedo adjustments are near zero everywhere in the fixed-T_s design (Figure 3b and 3n). In contrast they are large under fixed-SST (Figure 3a and 3m). Hence both of these adjustments (globally and regionally) in the fixed-SST ERF experimental design are principally the result of land warming (Figure 2b and Figures 3a-c,m-o). Fixing land temperatures has no impact on the stratospheric temperature adjustment (A_{strat}), consistent with this stratospheric process being largely decoupled from the troposphere (Table 1 and Figure 2b).

The roles of tropospheric temperature, water vapour and cloud adjustments are more complex. We begin by describing the changes under fixed-T_s. Figure 4a-c shows the change in zonal-mean temperature for 4xCO_2. Under fixed-T_s (Figure 4b), the reduced atmospheric radiative cooling from increased CO_2 results in a small warming of the free troposphere except in the mid to upper tropical troposphere which cools. Contrasting this with 4xCO_2-rad (Figure 4e) reveals the cooling to be the result of CO_2 stomatal effects, since 4xCO_2-rad warms throughout this region. We suggest that this is because – even though T_s is fixed – the increased CO_2 results in a reduced plant stomatal opening which forces a reduction in evapotranspiration from the surface (Section 2.1), potentially cutting off a source of moisture and condensational heating of the upper tropical troposphere. This is

consistent with observed large reductions in high level cloud fraction (defined below) in the 4xCO_2 fixed-T_s simulations over the Amazon and central African rainforests (Figure 5e) where CO_2 stomatal effects are expected to be largest. These high cloud reductions are not seen in the 4xCO_2-rad experiment (not shown).

Widespread free tropospheric warming in the 4xCO2 fixed-T_s experiment above a fixed surface (Figure 4b) reduces the atmospheric lapse-rate leading to a negative lapse-rate adjustment (A_{LR}) in most regions (and the global-mean, A_{LR}=-0.18 Wm^{-2}) except in the tropics which is affected by the stomatal effect described above (Figure 3h). In contrast, without CO_2 stomatal effects (the 4xCO_2-rad experiment) the free tropospheric warming persists everywhere (Figure 4e) and so reduces the tropospheric lapse-rate to a greater extent and increases emission to space everywhere (lapse-rate adjustment, -0.64 Wm^{-2}, Table 1 and Figure S1h).

The radiative effect of water-vapour change (A_q) largely follows the upper tropical tropospheric temperature change (Held and Soden, 2000) and we see this in our ERF experimental designs too. As described above, under 4xCO_2 fixed-T_s, there is upper tropical tropospheric cooling and consequently we find the water-vapour adjustment is negative (A_q=-0.17 Wm^{-2}). In contrast, in the 4xCO_2-rad experiment the water-vapour adjustment is positive (A_q=0.18 Wm^{-2}) due to free tropospheric warming everywhere (Figure 4e).

Figures 5d-l show the change in high-, mid- and low-level cloud fractions in the 4xCO_2 experimental designs, defined here as the maximum value of the area cloud fraction between 111m to 1949m (low level), 1949m to 5574m (mid level) and 5574 to 13608m (high level), i.e. assuming maximum overlap. While these cloud diagnostic changes may not be as well tied to TOA radiative flux changes as other cloud diagnostics (e.g. ISCCP simulator output) (Zelinka et al., 2012) they are indicative of large-scale cloud changes in the model. The warming of the free troposphere in the fixed-T_s designs results in large reductions in mid-level cloud fraction (Figure 5h). Under fixed-T_s there are also large reductions in low level continental clouds (Figure 5k) and consequently large positive cloud adjustments (A_c) over land (Figure 3q). These are not present in 4xCO_2-rad (Figure S1q) and hence are the result of CO_2 stomatal effects reducing boundary layer humidity and cloudiness (see Doutriaux-Boucher et al., 2009; Andrews et al., 2011; Arellano et al., 2011; Andrews and Ringer, 2014) independent of CO_2 stomatal effects on surface temperature (see below).

In contrast to the fixed-T_s results, under fixed-SST, a large land-sea contrast emerges (Figure 3 and 5). The addition of land surface warming results in large low level atmospheric stability reductions over land (Figure 5a,c crudely defined here as the change in 700mb temperatures minus surface temperatures) and the free tropospheric lapse-rate increases (i.e. a positive lapse-rate forcing adjustment over land, Figure 3g,i) accompanied with low level cloud reductions (Figure 5j) which increase the ERF (Figure 3p). Over the ocean, the land surface warming spreads out aloft (Figure 4a,c) above an unchanged ocean surface, resulting in large stability increases (Figure 5a,c) and lapse-rate reductions (i.e. a negative lapse-rate forcing adjustment, Figure 3g). The positive global-mean lapse-rate adjustment arising from land surface warming is enough to offset the negative lapse-rate adjustment under fixed-T_s, leaving a near zero global-mean lapse-rate adjustment in the fixed-SST design (Table 1) in this instance, but with a strong compensating land-sea contrast (Figure 3g)

Since marine low clouds are well understood to depend on changes in lower tropospheric stability (e.g., Klein and Hartmann 1993; Qu et al. 2015) there are large increases in marine low cloud fractions in response to land warming which reduce the ERF (i.e. a negative cloud adjustment), particularly in the tropical marine stratocumulus decks and transition to trade-cumulus (Figure 3p,r and Figure 5a,j). The geographical distribution of this cloud adjustment to land warming closely

resembles many of the geographical features in the total ERF difference between the fixed-SST and fixed-T_s designs (i.e. the land effect, Figure 1f). These large-scale land-sea processes are consistent with a shift in strong ascent and deep convention from ocean to land in response to land warming (e.g. Wyant et al., 2012). Indeed, Chadwick et al. (2019) looked at the circulation, precipitation and moisture convergence changes in response to land warming in these same experiments and found them consistent with such land-sea shifts with pressure at mean sea-level reducing over land and increasing over much of the Pacific (see their Figure 5f), driving low-level convergence over land.

Land warming in the 4xCO_2 fixed-SST ERF design therefore modifies the ERF via the following mechanisms: (i) reduces ERF via increased emission to space from surface and tropospheric warming ($A_{Planck_{surf}}$+$A_{Planck_{trop}}$+A_{LR} =-1.35 Wm^{-2}, Table 1), (ii) increases ERF due to water-vapour increases (A_q=0.49 Wm^{-2}), (iii) increases ERF due to land snow cover and surface albedo reductions (A_α=0.17 Wm^{-2}) and (iv) reduces ERF due to land-sea stability changes that alter cloudiness (global-mean cloud adjustments A_c=-0.26 Wm^{-2}). The sum is to reduce the 4xCO_2 fixed-SST ERF by ~1.0 Wm^{-2}, compared to an ERF with fixed-T_s. The above four terms are smaller in the 4xCO_2-rad simulation, summing to ~0.4 Wm^{-2}, suggesting a comparable role for CO_2 stomatal effects in driving land temperature change and atmospheric adjustments in response to CO_2 change in this model.

The 4xCO_2 stomatal effect in the fixed-T_s simulations gives rise to an ERF adjustment of ~0.8 Wm^{-2} (difference between 4xCO_2 and 4xCO_2-rad fixed-T_s ERF, Table 1), which is ~ 10% of the total 4xCO_2 fixed-T_s ERF. As noted previously, this principally arises because of cloud adjustments (~0.7 Wm^{-2}, i.e. the difference in fixed-T_s cloud adjustment in 4xCO_2 (0.80 Wm^{-2}) and 4xCO_2-rad (0.12 Wm^{-2}), Table 1) which arise in response to reduced evapotranspiration and so reduced boundary layer humidity and cloudiness (see Doutriaux-Boucher et al., 2009; Andrews et al., 2011; Arellano et al., 2011; Andrews and Ringer, 2014). In the fixed-SST simulations there are additional effects from land surface temperatures which both respond to these adjustments and are directly forced by the reduction in evapotranspiration, leading to increased surface temperatures via reduced evaporative cooling and changes in the bowen ratio, as seen in many studies (e.g. Boucher et al., 2009; Cao et al., 2009; Dong et al., 2010; Andrews and Ringer, 2014; Zarakas et al., 2020). Indeed, the difference in ΔT between 4xCO_2 and 4xCO_2-rad in the fixed-SST simulations is 0.16 K (Table 1). This land surface warming drives (negative) Planck and cloud responses (as described previously) that offset some of the fixed-T_s CO_2 stomatal effects. Hence in the fixed-SST design, the 4xCO_2 stomatal effect is somewhat smaller, at 0.24 Wm^{-2}, because of compensating land surface warming effects and adjustments.

Finally, to check the robustness of the basic physical mechanisms (i.e. excluding the stomatal effects) described in this Section (e.g. the large-scale stability, land-sea contrasts and cloud changes), we compare the land warming effect in the 4xCO_2-rad simulation to the +Solar ERF simulation (note that the +Solar experiment has a similar in magnitude ERF to 4xCO_2-rad, Table 1, which aids the comparison). Both give rise to a total land warming effect of the order -0.4 Wm^{-2}. The surface and tropospheric Planck, water-vapour and cloud adjustment components to the land warming are all extremely similar (Table 1) including their geographic distributions (Figures S1 and S2). The one exception perhaps is the lapse-rate component, which have a similar geographical pattern of opposing land-sea terms (Figures S1i and S2i) but cancel to +0.09 Wm^{-2} in the global-mean response to solar forcing but +0.25 Wm^{-2} in 4xCO_2-rad (Table 1). We do not pursue this further, but speculate that differences in the geographical distribution of CO_2 versus solar forcing might lead to different patterns in land surface warming and different vertical profiles (Figure 4d-i), and so how the warming is spread more widely across the tropical oceans (Chadwick et al., 2019).

4. Methods used to account for land temperature change

With ERFs calculated with both fixed-SST and fixed-T_s experimental designs we are now in a position to test the various methods described in the Introduction that have been proposed to correct for the radiative effect of land warming in fixed-SST ERF experiments.

4.1. Feedback parameter correction method

The feedback parameter method proposed by Hansen et al. (2005) assumes the radiative effect of land warming in the fixed-SST experiment can be calculated by scaling the global-mean surface-air-temperature change, ΔT=0.56 K (Table 1), with the model's feedback parameter (λ) derived from long-term coupled GCM climate sensitivity experiments. We assume λ = -0.78 Wm^{-2} K^{-1} for ACCESS1.0 derived from CMIP5 abrupt-4xCO_2 coupled Atmosphere-Ocean GCM (AOGCM) simulations (Forster et al., 2013), thus giving a land warming effect of $\lambda\Delta T$ = -0.78 Wm^{-2} K^{-1} x 0.56 K =-0.44 Wm^{-2}, just less than half of the ~-1.0 Wm^{-2} found in Section 3. Or put another way, correcting the fixed-SST 4xCO_2 ERF (7.03 Wm^{-2}, Table 1) for land temperature change with this correction method gives a corrected forcing of 7.03+0.44=7.47 Wm^{-2}, substantially less than the 7.98 Wm^{-2} simulated by the model with fixed-T_s (a comparison is presented in Figure 6).

A caveat to this calculation is that the CMIP5 ACCESS1.0 configuration analysed in Forster et al. (2013) (from which we have assumed the coupled model's long-term λ) is not identical to that used here, but even the entire CMIP5 λ distribution, λ = -1.13 (-0.62 to -1.64) [multi-model mean; 5-95%] Wm^{-2} K^{-1} (Forster et al. 2013), only generates a radiative effect of -0.63 [-0.35 to -0.92] Wm^{-2}. Smith, Kramer and Myhre et al. (2020) similarly applied the feedback parameter correction method to CMIP6 experiments and found a radiative effect of -0.48 ± 0.29 [5-95%] Wm^{-2} across models, which is similar to that seen here.

The reason the feedback parameter method is found to be insufficient is that λ derived from a long-term coupled climate change simulations (where both SST and land temperatures evolve together) is inadequate for explaining the radiative response to a global temperature change that arises solely from land temperature change. That is, the land effect in the fixed-SST experiment gives a radiative effect per unit ΔT of ~-0.95 Wm^{-2} / 0.43 K = -2.21 Wm^{-2} K^{-1} (Table 1, 4xCO_2 'land effect' row), which is much more stabilizing than the feedback parameter seen in ACCESS1.0 (or GCMs in general) 4xCO_2 climate sensitivity experiments (Zelinka et al. 2020). Using λ calculations from earlier sections of 4xCO_2 runs – which tend to be more stabilizing (e.g. Andrews et al. 2015) – may improve this method. However even using the first 20 years of abrupt-4xCO_2 still only gives λ=-1.08 Wm^{-2} K^{-1} for ACCESS1.0 (Andrews et al. 2015) and so a land warming radiative effect of -0.60 Wm^{-2}.

To identify which processes are responsible for the larger TOA radiative response per unit ΔT in response to land warming, we compare the individual adjustment terms (normalised by ΔT) to the analogous radiative feedback terms from Zelinka et al. (2020). Zelinka et al. (2020) report the long-term abrupt-4xCO_2 ACCESS1.0 AOGCM individual feedback terms as Planck (-3.23 Wm^{-2} K^{-1}), lapse-rate (-0.42 Wm^{-2} K^{-1}), water-vapour (1.77 Wm^{-2} K^{-1}), surface albedo (0.47 Wm^{-2} K^{-1}) and cloud (0.40 Wm^{-2} K^{-1}). In contrast, here we find the normalised Planck adjustment to land warming to be slightly stronger in magnitude ($A_{Planck}/\Delta T$ = ($A_{Planck_{surf}}$+$A_{Planck_{trop}}$)/ΔT = -1.54 Wm^{-2}/0.43 K = -3.58 Wm^{-2} K^{-1}, Table 1, 4xCO_2 'land effect' row) and the surface albedo response slightly weaker ($A_\alpha/\Delta T$ = 0.17 Wm^{-2}/0.43 K = 0.40 Wm^{-2} K^{-1}), presumably in part because there is no sea-ice response in the ERF experiments. Both make the TOA radiative response per unit ΔT larger for land warming than when the land and oceans warm together. However much bigger differences are observed in the lapse-rate, water-vapour and cloud terms. For the lapse-rate, as described in Section 3.2 and shown in

Figure 3i, A_{LR} is positive over land where there is strong surface warming, and negative over oceans where warming spreads out at upper levels above an unchanged surface (reducing the atmospheric lapse-rate). The global-mean lapse-rate adjustment is overall positive, and so the normalised response ($A_{LR}/\Delta T$ = 0.19 Wm^{-2}/0.43 K = 0.44 Wm^{-2} K^{-1}) is of opposite sign to the negative lapse-rate feedback seen in the AOGCM 4xCO_2 simulation. This is largely compensated for by a much weaker water-vapour response ($A_q/\Delta T$ = 0.49 Wm^{-2}/0.43 K = 1.14 Wm^{-2} K^{-1}). We do not pursue these differing lapse-rate and water-vapour responses to land and ocean warming further, but suggest that the larger lapse-rate response to ocean warming is simply the result of the unlimited moisture source which permits the maintenance of a moist-adiabat under warming, unlike the response to land surface warming where moisture availability is limited (see Joshi et al., 2008). As discussed in Section 3.2 and seen in Figure 3r, the global cloud response is negative in response to land warming because of increased marine cloudiness ($A_c/\Delta T$ = -0.26 Wm^{-2}/0.43 K = -0.60 Wm^{-2} K^{-1}), whereas it is strongly positive in 4xCO_2 ACCESS1.0 AOGCM simulations where reductions in marine cloudiness are expected (+0.40 Wm^{-2} K^{-1}, Zelinka et al., 2020). That radiative responses to surface temperature change – in particular cloud and lapse-rate responses – are found to strongly depend on the pattern of temperature change, is not unexpected and consistent with previous studies (e.g. Andrews et al., 2015; Rugenstein et al. 2016; Zhou et al., 2016; Andrews and Webb, 2018).

Applying the feedback correction method to the 4xCO_2-rad fixed-SST ERF gives a land warming effect of $\lambda\Delta T$ = -0.78 Wm^{-2} K^{-1} x 0.40 K = -0.31 Wm^{-2}, which is again smaller than the radiative effect of land warming found in this experiment in Section 3 and Table 1. Similarly, applied to the +Solar fixed-SST ERF gives a land warming effect of $\lambda\Delta T$ = -0.78 Wm^{-2} K^{-1} x 0.25 K = -0.20 Wm^{-2}, which is again about half of the radiative effect of land warming found in this experiment (Section 3 and Table 1).

In principle one could also apply the method regionally to estimate a spatial pattern of the land warming correction term. The result ought to look like Figure 1f (i.e. the spatial pattern of the ERF land effect), which as previously noted resembles many of the geographical features of the cloud adjustment (Figure 3r) – particularly over the ocean. To apply the feedback correction method regionally one could simply scale a model's regional feedback parameter by the global-mean ΔT from the fixed-SST experiment, analogous to the above global-mean results. In practice however estimating the spatial pattern of an individual model's feedback pattern can be noisy without an ensemble of AOGCM abrupt-4xCO_2 simulations. Moreover Andrews et al. (2015; their Figure 5) show the spatial pattern of the CMIP5 multi-model mean feedback parameter in response to land and ocean warming in abrupt-4xCO_2 AOGCM simulations to include many more processes and features than seen here in response to just land warming (e.g. Figure 1f and Figure 3). Therefore we suggest that scaling a model's regional feedback parameter derived from experiments where land and ocean warm together will not be able to reproduce the desired spatial pattern of the ERF correction term.

4.2. Surface temperature correction method

The surface temperature method applied in Smith, Kramer and Myhre et al. (2020) assumes the radiative effect of the surface temperature change only (i.e. the surface Planck adjustment). This is -0.48 Wm^{-2} in the fixed-SST 4xCO_2 experiment (Table 1), again about half of the required total correction. Correcting the fixed-SST 4xCO_2 ERF for land temperature change with this correction method gives a corrected forcing of 7.03+0.48=7.51 Wm^{-2}, again substantially less than that simulated by model with fixed-T_s (Figure 6).

Similarly, Smith, Kramer and Myhre et al. (2020) applied this correction method to CMIP6 4xCO_2 fixed-SST ERF experiments and found it to be -0.43 ± 0.09 [5-95%] Wm^{-2} across models. This underestimate of the land effect arises simply because the method ignores the other adjustments to land warming which we have shown to be important. Applied to 4xCO_2-rad and Solar, the surface temperature method gives -0.35 Wm^{-2} and -0.26 Wm^{-2} respectively, which goes further in explaining the total -0.4 Wm^{-2} land warming effect. However, that it explains a larger fraction of the total effect is due to fortuitous cancellations in the other adjustment terms (Table 1).

Applying this method regionally simply results in a correction term equal to the spatial pattern of the surface Planck adjustment in the fixed-SST experiment (Figure 3a). While this may produce a reasonable correction pattern over land (contrasting to Figure 1f) it clearly misses desired large-scale patterns over the ocean by construction.

4.3. Tropospheric and surface correction method

The tropospheric and surface correction method applied by Tang et al. (2019) assumes various adjustments from the fixed-SST experiment that can reasonably be assumed to be related to the land warming. That is, we sum the surface (-0.48 Wm^{-2}) and tropospheric Planck adjustment (-1.15 Wm^{-2}) (i.e. what Tang et al., 2019, describe as a constant tropospheric lapse rate term), a corresponding fraction of the water-vapour adjustment (as calculated below) and the surface albedo (+0.15 Wm^{-2}) adjustment from the fixed-SST experiment. The water vapour adjustment corresponding to the assumed vertically uniform warming is determined by scaling the water-vapour adjustment in the fixed-SST experiment by the fraction of the tropospheric Planck adjustment (i.e. vertically uniform) to the full tropospheric temperature adjustment (i.e. $A_{Planck_{trop}}/(A_{LR}+ A_{Planck_{trop}})$) (Tang et al., 2019). Applied to Table 1 this gives a scaling close to unity (or even positive), and so has little impact on the water-vapour adjustment (+0.32 Wm^{-2}). This arises because A_{LR} in the denominator is positive (or near zero) owing to the CO_2 stomatal effect described in Section 3.2. Hence in this instance the method successfully predicts that the water-vapour adjustment to land warming is larger than the water-vapour adjustment seen in the fixed-SST experiment. In contrast, in 4xCO_2-rad and Solar, A_{LR} is substantially negative and so the scaling is < 1, and again the method correctly predicts the water-vapour adjustment to land warming is smaller than that seen in the fixed-SST experiment (Table 1). However in all instances it underestimates this difference.

Applying the method to the 4xCO_2 fixed-SST adjustments in Table 1 gives a land radiative effect of -1.16 Wm^{-2}. Correcting the fixed-SST 4xCO_2 ERF for land temperature change with this correction method gives a corrected forcing of 7.03+1.16=8.19 Wm^{-2}. This time a slight overestimate but an improvement on the previous two methods (Figure 6) because it accounts for some tropospheric responses which are clearly caused by land warming. Applying the method to 4xCO_2-rad and Solar gives a land temperature effect of -0.67 Wm^{-2} and -0.33 Wm^{-2} respectively. The method cannot be exact because it ignores the role of cloud and lapse rate changes in response to land warming which we have shown to be important terms – at least in ACCESS1.0.

Tang et al. (2019) applied the method to nine PDRMIP (Myhre et al. 2017) models forced by CO_2 doubling (2xCO_2) and found a mean radiative effect from land warming (scaled to 4xCO_2, assuming a logarithmic relationship with CO_2 concentration) of -0.96 (0.64 to 1.28) Wm^{-2} [5-95%] compared to fixed-SST values. Similarly, Smith, Kramer and Myhre et al. (2020) applied the method (in addition to the surface temperature correct method of the previous section) to CMIP6 4xCO_2 fixed-SST ERF experiments and found an effect of -0.86 ± 0.35 [5-95%] Wm^{-2}. These values are again close to the values simulated by ACCESS1.0.

As in Section 4.1 and 4.2 we could in principle also apply this method regionally. This would require summing the spatial patterns of the Planck surface (Figure 3a), Planck troposphere (Figure 3d), surface albedo (Figure 3m) and a fraction of water vapour (Figure 3j) from the fixed-SST experiments. However, like for the previous methods, it is clear that this cannot result in the desired ERF correction to land warming over the oceans since the method does not account for cloud and lapse-rate change (which are the principle adjustments to land warming that have remote oceanic effects, Figure 3).

In summary, the tropospheric and surface correction method applied by Tang et al. (2019) to PDRMIP models and Smith, Kramer and Myhre et al. (2020) to CMIP6 simulations appears to correct well for the change in surface land temperature, albedo, and tropospheric temperatures in the fixed-SST simulations. It is an approximation for the water vapour change but does not include any correction for lapse-rate and cloud changes caused by land warming (both of which have large local and remote effects over the oceans).

5. Summary and discussion

A self-consistent forcing-feedback framework requires forcing and adjustments to be separated from feedback by identifying radiative responses that are not mediated by global-mean surface-air-temperature change, ΔT (Shine et al., 2003; Hansen et al., 2005; Sherwood et al., 2015; 2020). In practice however, ERF is typically calculated in GCMs with fixed sea-surface-temperatures and sea-ice fraction (e.g. Myhre et al., 2013; Forster et al., 2016), and so land temperatures are free to respond and so some ΔT and radiative effects arise that might be better considered a feedback and so contaminate the ERF estimate. Here we have calculated the ERF from $4xCO_2$ in a complex GCM with both fixed-SST and fixed land and SST (fixed-T_s) for the first time. This allows a separation of those responses that occur due to reduced atmospheric radiative cooling from those that occur due to land warming in the fixed-SST design.

With fixed-SSTs, the $4xCO_2$ ERF is 7.0 Wm^{-2}, compared to 8.0 Wm^{-2} when surface temperatures are fixed globally (fixed-T_s). This difference (-1 Wm^{-2}) arises due to the influence of land warming in fixed-SST ERF design. The contribution from CO_2 stomatal effects are also quantified and found to contribute just over half of the radiative effect of land warming and associated radiative adjustments. We expect some 'physical' responses associated with land warming in the fixed-SST experimental design to be robust, such as increased emission to space from surface and atmospheric warming, and reduced outgoing SW radiation from reduced snow-cover / surface albedo. Land warming also drives large-scale land-sea circulation and stability changes such as a shift in deep convection from ocean to land (e.g. Wyant et al., 2012) associated with low pressure and low-level land convergence (Chadwick et al., 2019). The land surface warming spreads out aloft through the free troposphere, increasing lower tropospheric stability over the oceans and increasing low-level marine cloudiness.

Our results are from a single GCM and the quantitative radiative effects will likely vary considerably across GCMs owing to different atmospheric parameterisations and land surface schemes, especially given the important contribution we have found from CO_2 plant stomatal effects as these are not well constrained (e.g. Fisher et al. 2018). In particular we found a $4xCO_2$ stomatal effect in the fixed-T_s simulations of ~0.8 Wm^{-2}, which is ~10% of the total $4xCO_2$ fixed-T_s ERF. This principally arose because of a cloud adjustment to the reduced evapotranspiration, which reduces boundary layer

humidity and cloudiness (see also Doutriaux-Boucher et al., 2009; Andrews et al., 2011; Arellano et al., 2011; Andrews and Ringer, 2014). In the fixed-SST simulations the stomatal effect is smaller (0.24 Wm^{-2}) because of the radiative effect of increased land surface temperature and associated adjustments which offsets a large part of the fixed-T_s CO_2 stomatal adjustments. There are limited studies to contrast these CO_2 stomatal effects on ERF against, and none with the fixed-T_s experimental design used here. The fixed-SST 4xCO_2 stomatal effect agrees with a value reported in Andrews et al. (2012a) (they found an adjustment of 0.25 Wm^{-2}), but this is expected since they used the HadGEM2-ES model which shares the same atmospheric physics and land surface scheme as ACCESS1.0. While not specifically quantifying ERF, Arora et al. (2013) and Zarakas et al. (2020) showed a large model spread in CMIP5 and CMIP6 surface temperature responses to CO_2 plant physiological effects in coupled AOGCM 1%CO_2 increase experiments. HadGEM2-ES was identified as having a particularly large response compared to other models (see for example Table 2 of Zarakas et al., 2020). Given the similarities of HadGEM2-ES and ACCESS1.0, it is possible that the CO_2 stomatal effects in ACCESS1.0 could also be large. On the other hand, Andrews et al. (2012b) showed that many CMIP5 GCMs simulate a global-mean surface-air-temperature change, ΔT, of ~0.5K in 4xCO_2 fixed-SST ERF simulations (see their Figure 1, red crosses) which is comparable to the 0.56K simulated here with ACCESS1.0. Hence – at least in the fixed-SST ERF experimental design – the land surface temperature change in ACCESS1.0 is not unusual.

The experimental designs used here are useful for understanding and evaluating effective radiative forcing and the physical mechanisms of forcing adjustments. In response to increased CO_2 we are able to separate adjustments associated with (i) reduced atmospheric radiative cooling (i.e. the direct radiative effect), (ii) land surface warming and (iii) plant stomatal-evapotranspiration effects. We have shown that all generate important processes and need to be considered when evaluating ERF. For example Kamae et al. (2019) found that in response to increased CO_2, the reduced atmospheric radiative cooling and the effects of land warming in a 4xCO_2 fixed-SST experiment were comparably important in driving marine low cloud adjustments over the cool (<27^{o}C) oceans. This implies many aspects of adjustments seen in fixed-SST ERF experiments may not be unique to a specific forcing agent, but common to all forcing agents through the experimental design of allowing land surface temperatures to change.

An alternative experimental framework for estimating ERF with no land surface temperature change are aquaplanets whereby a climate model's ocean, land and sea-ice are replaced with fixed SSTs (e.g. Mediros et al. 2015; Mediros, 2020). While aquaplanets contain other simplifications (such as being zonally-symmetric and having no seasonal cycle) our results suggest imply that the magnitude of ERF ought to be greater in aquaplanets relative to AMIP type fixed-SST experiments, due to the lack of a land response and associated adjustments in the aquaplanets. Indeed, both Ringer et al. (2014) and Mediros et al. (2015) show this to be the case across CMIP5 aquaplanet and AMIP 4xCO_2 ERF experiments, and Mediros (2020) show it to be true for an aerosol ERF. Aquaplanets have been shown to be a useful configuration in the hierarchy of models for understanding processes that drive climate change (e.g. Mediros et al. 2015; Mediros, 2020). We suggest our AMIP type ERF experiment with fixed SST and land provides a stepping stone between the simplified aquaplanet and more complex AMIP type fixed-SST ERF configurations in this hierarchy.

We have shown the radiative effect of land warming in fixed-SST ERF experiments is -1.0 Wm^{-2} (~14% of the total ERF) in ACCESS1.0 for 4xCO_2 and -0.4 Wm^{-2} (~6%) when the warming from CO_2 stomatal effects are omitted or when forced with an increase in the solar constant. Previous methods (Hansen et al. 2005; Tang et al., 2019; Richardson et al., 2019; Smith, Kramer and Myhre et al., 2020) proposed to account for land warming effects in fixed-SST ERF estimates were tested

against our results and none were able to robustly predict the land warming effect across all of our ERFs globally or spatially. However we suggest the tropospheric and surface correction method applied by Tang et al. (2019) is most closely related to the underlying physical processes and its assumptions are generally borne out in our GCM results. For example, it correctly accounts for the change in surface land temperature, albedo, and an aspect of tropospheric temperature change in the fixed-SST simulations caused by the land warming. It approximates a component of associated water vapour change but does not include any correction for lapse-rate and cloud changes caused by land warming. Further work refining these methods, globally and regionally, and incorporating lapse-rate and cloud changes to land warming would be useful.

By holding SST and land surface temperatures fixed in an ERF experiment we have provided one definition of an ERF with zero global-mean surface-air-temperature change, ΔT, that would satisfy the classical forcing-feedback paradigm (Sherwood et al., 2015; 2020). However such a state with global-mean ΔT=0 is not uniquely defined. Indeed, the commonly used Gregory-type regression method to estimate ERF (Gregory et al. 2004) also provides an example of an ERF defined with zero global-mean temperature change, but without constraint on *local* surface temperature change. Andrews et al (2015) showed that Gregory-type regression estimates of ERF include the effect of a rapid adjustment in local surface temperature change (with zero global-mean). They showed that, in response to $4xCO_2$, such a pattern of surface temperature change can give rise to a $4xCO_2$ ERF adjustment of ~-0.5 W m^{-2}. Since local surface temperature adjustments are included in the ERF estimated by the Gregory-type regression method (requiring only zero global-mean temperature change) but excluded by our fixed-T_s method (requiring zero local temperature change), these two definitions are in principle different (Andrews et al. 2015) but both would satisfy the forcing-feedback paradigm which is only defined with respect to global-mean ΔT. In our comparison of methods to account for land warming in fixed-SST ERF estimates, we have evaluated against a definition of ERF that requires zero local temperature change, in addition to the global-mean. One could – in principle – argue that the proposed correction methods simply result in alternative definitions of ERF.

As the radiative effects of land warming are likely to depend on GCM physics (e.g. cloud parameterisations, land surface schemes etc.) we are not able to recommend a definitive correction for land warming effects in fixed-SST GCM experiments. To potentially bound this issue – whilst acknowledging the limitation that there might not be a unique way of prescribing land properties in GCMs (Hansen et al., 2005; Ackerley et al. 2018) - it would be useful if other modelling centres performed similar experiments in an attempt to quantify this structural uncertainty.

Data Availability Statement

The Prescribed Land AMIP (PLAMIP) v1.0 dataset is available through Ackerley et al. (2018).

Acknowledgements

We thank Steve Klein for helpful discussions related to land warming in fixed-SST simulations. We also thank Steve Sherwood and two anonymous reviewers for helpful comments. TA and DA were supported by the Met Office Hadley Centre Climate Programme funded by Department for Business, Energy and Industrial Strategy (BEIS) and Department for Environment, Food and Rural Affairs (Defra). TA, CJS, GM and PMF were supported by the European Union's Horizon 2020 research and innovation programme under grant agreement No 820829 (CONSTRAIN project). CJS was supported

by a NERC/IIASA Collaborative Research Fellowship (NE/T009381/1). RC was supported by the Newton Fund through the Met Office Climate Science for Service Partnership Brazil (CSSP Brazil).

References

Ackerley, D., Chadwick, R., Dommenget, D., & Petrelli, P., 2018: An ensemble of AMIP simulations with prescribed land surface temperatures. *Geoscientific Model Development*, 11(9), 3865– 3881. doi: 10.5194/gmd-11-3865-2018.

Ackerley, D., & Dommenget, D. (2016). Atmosphere-only GCM (ACCESS1.0) simulations with prescribed land surface temperatures. *Geoscientific Model Development*, 9(6), 2077– 2098, doi: 10.5194/gmd-11-3865-2018.

Andrews, T., and M. J. Webb, 2018: The Dependence of Global Cloud and Lapse Rate Feedbacks on the Spatial Structure of Tropical Pacific Warming. *J. Climate*, 31, 641–654, doi: 10.1175/JCLI-D-17-0087.1.

Andrews, T., J.M. Gregory and M.J. Webb, 2015: The dependence of radiative forcing and feedback on evolving patterns of surface temperature change in climate models. *J. Climate*, 28, 1630-1648, doi:10.1175/JCLI-D-14-00545.1.

Andrews, T., and M.A. Ringer, 2014: Cloud feedbacks, rapid adjustments, and the forcing-response relationship in a transient CO2 reversibility scenario. *J. Climate*, 27, 1799-1818, doi:10.1175/JCLI-D-13-00421.1

Andrews, T., Ringer, M. A., Doutriaux-Boucher, M., Webb, M. J., and Collins, W. J., 2012a: Sensitivity of an Earth system climate model to idealized radiative forcing, *Geophys. Res. Lett.*, 39, L10702, doi: 10.1029/2012GL051942.

Andrews, T., Gregory, J. M., Webb, M. J., and Taylor, K. E., 2012b: Forcing, feedbacks and climate sensitivity in CMIP5 coupled atmosphere-ocean climate models, *Geophys. Res. Lett.*, 39, L09712, doi: 10.1029/2012GL051607.

Andrews, T., M. Doutriaux-Boucher, O. Boucher and P.M. Forster, 2011: A regional and global analysis of carbon dioxide physiological forcing and its impact on climate. *Climate Dynamics*, 36:783-792, doi:10.1007/s00382-010-0742-1.

Arellano, J., van Heerwaarden, C., & Lelieveld, J. (2012). Modelled suppression of 4430 boundary-layer clouds by plants in a CO2-rich atmosphere. *Nat. Geosci.*, 5, 701-704. 4431 doi: 10.1038/ngeo1554.

Arora, V. K., and Coauthors, 2013: Carbon–Concentration and Carbon–Climate Feedbacks in CMIP5 Earth System Models. *J. Climate*, 26, 5289–5314, doi: doi.org/10.1175/JCLI-D-12-00494.1.

Best, M. J., Pryor, M., Clark, D. B., Rooney, G. G., Essery, R. L. H., Ménard, C. B., Edwards, J. M., Hendry, M. A., Porson, A., Gedney, N., Mercado, L. M., Sitch, S., Blyth, E., Boucher, O., Cox, P. M., Grimmond, C. S. B., and Harding, R. J., 2011: The Joint UK Land Environment Simulator (JULES), model description – Part 1: Energy and water fluxes, Geosci. Model Dev., 4, 677–699, doi: 10.5194/gmd-4-677-2011.

Bony, S., and Coauthors, 2006: How Well Do We Understand and Evaluate Climate Change Feedback Processes?. *J. Climate*, 19, 3445–3482, doi: 10.1175/JCLI3819.1.

Boucher, O., et al., 2013: Clouds and Aerosols. In: Climate Change 2013: The Physical Science Basis. Contribution of Working Group I to the Fifth Assessment Report of the Intergovernmental Panel on Climate Change. T.F. Stocker, et al., Eds. Cambridge University Press. Cambridge University Press.

Boucher, O., Jones, A. & Betts, R.A., 2009: Climate response to the physiological impact of carbon dioxide on plants in the Met Office Unified Model HadCM3. *Clim Dyn*, 32, 237–249. doi: 10.1007/s00382-008-0459-6

Bi, D., Dix, M., Marsland, S., O'Farrell, S., Rashid, H., Uotila, P., Hirst, T., Kowalczyk, E., Golebiewski, M., Sullivan, A., Yan, H., Hannah, N., Franklin, C., Sun, Z., Vohralik, P., Watterson, I., Zhou, X., Fiedler, R., Collier, M., Ma, Y., Noonan, J., Stevens, L., Uhe, P., Zhu, H., Griffies, S., Hill, R., Harris, C., & Puri, K. (2013). The ACCESS coupled model: Description, control climate and evaluation. *Australian Meteorological and Oceanographic Journal*, 63, 41– 64.

Cao, L., Bala, G., Caldeira, K., Nemani, R., and Ban-Weiss, G., 2009: Climate response to physiological forcing of carbon dioxide simulated by the coupled Community Atmosphere Model (CAM3.1) and Community Land Model (CLM3.0), *Geophys. Res. Lett.*, 36, L10402, doi:10.1029/2009GL037724.

Chadwick, R., D. Ackerley, T. Ogura & D. Dommenget, 2019: Separating the influences of land warming, the direct CO_2 effect, the plant physiological effect, and SST warming on regional precipitation changes. *JGR: Atmospheres*, 124, 624– 640, doi: 10.1029/2018JD029423.

Chadwick, R., Good, P., Andrews, T., & Martin, G., 2014: Surface warming patterns drive tropical rainfall pattern responses to CO_2 forcing on all timescales. *Geophysical Research Letters*, 41, 610–615, doi: 10.1002/2013GL058504.

Cox, P., Betts, R., Bunton, C. *et al.*, 1999: The impact of new land surface physics on the GCM simulation of climate and climate sensitivity. *Climate Dynamics*, 15**,** 183–203. doi: 10.1007/s003820050276.

Dong, B., J. M. Gregory, and R. T. Sutton, 2009: Understanding Land–Sea Warming Contrast in Response to Increasing Greenhouse Gases. Part I: Transient Adjustment. *J. Climate*, 22, 3079–3097, doi: 10.1175/2009JCLI2652.1.

Doutriaux-Boucher, M., Webb, M. J., Gregory, J. M., and Boucher, O., 2009: Carbon dioxide induced stomatal closure increases radiative forcing via a rapid reduction in low cloud, *Geophys. Res. Lett.*, 36, L02703, doi:10.1029/2008GL036273.

Essery, R. L. H., M. J. Best, R. A. Betts, P. M. Cox, and C. M. Taylor, 2003: Explicit Representation of Subgrid Heterogeneity in a GCM Land Surface Scheme. *J. Hydrometeor.*, 4, 530–543, doi: 10.1175/1525-7541(2003)004<0530:EROSHI>2.0.CO;2.

Field, C.B., Jackson, R.B. and Mooney, H.A., 1995: Stomatal responses to increased CO_2: implications from the plant to the global scale. *Plant, Cell & Environment*, 18: 1214-1225. doi:10.1111/j.1365-3040.1995.tb00630.x.

Fisher, RA, Koven, CD, Anderegg, WRL, et al., 2018: Vegetation demographics in Earth System Models: A review of progress and priorities. *Glob Change Biol*. 24: 35– 54. doi: 10.1111/gcb.13910.

Forster, P.M., T. Richardson, A.C. Maycock, C.J. Smith, B.H, Samset, G. Myhre, T. Andrews, R. Pincus and M. Schulz, 2016: Recommendations for diagnosing effective radiative forcing from climate models for CMIP6. *J. Geophys. Res. Atmos.*, 121, 12, 460-12,475, doi: 10.1002/2016JD025320.

Forster, P.M., T. Andrews, P. Good, J.M. Gregory, L.S. Jackson and M. Zelinka, 2013: Evaluating adjusted forcing and model spread for historical and future scenarios in the CMIP5 generation of climate models. *J. Geophys. Res.*, 118, 1139-1150, doi:10.1002/jgrd.50174.

Gates, W. L., and Coauthors, 1999: An Overview of the Results of the Atmospheric Model Intercomparison Project (AMIP I). *Bull. Amer. Meteor. Soc.*, 80, 29–56, doi: 10.1175/1520-0477(1999)080<0029:AOOTRO>2.0.CO;2.

Gregory, J. M., Ingram, W. J., Palmer, M. A., Jones, G. S., Stott, P. A., Thorpe, R. B., Lowe, J. A., Johns, T. C., and Williams, K. D., 2004: A new method for diagnosing radiative forcing and climate sensitivity, *Geophys. Res. Lett.*, 31, L03205, doi: 10.1029/2003GL018747.

Hansen, J., et al. (2005), Efficacy of climate forcings, *J. Geophys. Res.*, 110, D18104, doi:10.1029/2005JD005776.

Held, I.M., and B.J. Soden, 2000: Water Vapor Feedback and Global Warming. *Annual Review of Energy and the Environment*, 441-475.

Joshi, M.M., Gregory, J.M., Webb, M.J. *et al.*, 2008: Mechanisms for the land/sea warming contrast exhibited by simulations of climate change. *Clim Dyn*, 30, 455–465, doi: 10.1007/s00382-007-0306-1.

Kamae, Y., R. Chadwick, D. Ackerley, M. Ringer and T. Ogura, 2019: Seasonally variant low cloud adjustment over cool oceans. *Clim. Dyn.*, 52, 5801-5817. doi:10.1007/s00382-018-4478-7.

Klein, S. A., and D. L. Hartmann, 1993: The Seasonal Cycle of Low Stratiform Clouds. *J. Climate*, 6, 1587–1606.

Kowalczyk, Eva & Stevens, & Law, & Dix, Martin & Wang, Yingping & Harman, Ian & Haynes, & Srbinovsky, & Pak, B. & Ziehn, T., 2012: The land surface model component of ACCESS: Description and impact on the simulated surface climatology. Australian Meteorological and Oceanographic Journal. AMOJ. 65-82. 10.22499/2.6301.005.

Kowalczyk, E. A., Stevens, L., Law, R. M., Dix, M., Wang, Y. P.,Harman, I. N., Haynes, K., Srbinovsky, J., Pak, B., and Ziehn,T., 2013: The land surface model component of ACCESS: description and impact on the simulated surface climatology, Aust. Meteorol. Ocean. J., 63, 65–82. doi: 10.22499/2.6301.005.

Martin, G., et al., 2011: The HadGEM2 family of Met Office Unified Model climate configurations, *Geosci. Model Dev.*, 4, 723–757, doi: 10.5194/gmd-4-723-2011.

Medeiros, B., 2020: Aquaplanets as a framework for examination of aerosol effects. *Journal of Advances in Modeling Earth Systems*, 12, e2019MS001874. doi: 10.1029/2019MS001874.

Medeiros, B., Stevens, B. & Bony, S., 2015: Using aquaplanets to understand the robust responses of comprehensive climate models to forcing. *Clim Dyn*, 44, 1957–1977, doi: 10.1007/s00382-014-2138-0.

Myhre, G., et al., 2013: Anthropogenic and natural radiative forcing. In Climate Change 2013: The Physical Science Basis. Contribution of Working Group I to the Fifth Assessment Report of the Intergovernmental Panel on Climate Change. T.F. Stocker, et al., Eds. Cambridge University Press, pp 659-740.

Myhre, G., and Coauthors, 2017: PDRMIP: A Precipitation Driver and Response Model Intercomparison Project—Protocol and Preliminary Results. *Bull. Amer. Meteor. Soc.*, 98, 1185–1198, doi: 10.1175/BAMS-D-16-0019.1.

Pincus, R., Forster, P. M., and Stevens, B., 2016: The Radiative Forcing Model Intercomparison Project (RFMIP): experimental protocol for CMIP6, Geosci. Model Dev., 9, 3447–3460, doi: 10.5194/gmd-9-3447-2016.

Qu, X., Hall, A., Klein, S. A., and DeAngelis, A. M. (2015), Positive tropical marine low-cloud cover feedback inferred from cloud-controlling factors, *Geophys. Res. Lett.*, 42, 7767– 7775, doi:10.1002/2015GL065627.

Ramaswamy, V., and Coauthors, 2018: Radiative Forcing of Climate: The Historical Evolution of the Radiative Forcing Concept, the Forcing Agents and their Quantification, and Applications. *Meteor. Monogr.*, 2018; 59 14.1–14.101. doi: https://doi.org/10.1175/AMSMONOGRAPHS-D-19-0001.1.

Richardson, T. B., Forster, P. M., Smith, C. J., Maycock, A. C., Wood, T., Andrews, T., et al., 2019: Efficacy of climate forcings in PDRMIP models. *JGR*, 124, 12824– 12844. doi: 10.1029/2019JD030581.

Richardson, T. B., Forster, P. M., Andrews, T., & Parker, D. J., 2016: Understanding the rapid precipitation response to CO_2 and aerosol forcing on a regional scale. *Journal of Climate*, 29(2), 583–594, doi: 10.1175/JCLI-D-15-0174.1.

Ringer, M. A., Andrews, T., and Webb, M. J., 2014: Global-mean radiative feedbacks and forcing in atmosphere-only and coupled atmosphere-ocean climate change experiments, *Geophys. Res. Lett.*, 41, 4035– 4042, doi:10.1002/2014GL060347.

Rugenstein, M.A.A., K. Caldeira and R. Knutti, 2016: Dependence of global radiative feedbacks on evolving patterns of surface heat fluxes, *Geophys. Res. Lett.*, 43, 9877– 9885, doi: 10.1002/2016GL070907.

Sanderson, B.M., Shell, K.M. & Ingram, W., 2010: Climate feedbacks determined using radiative kernels in a multi-thousand member ensemble of AOGCMs. *Clim Dyn*, 35, 1219–1236, doi:10.1007/s00382-009-0661-1

Sherwood, S. C., et al., 2015: Adjustments in the forcing–feedback framework for understanding climate change. *Bull. Amer. Meteor. Soc.*, 96, 217–228, doi: 10.1175/BAMS-D-13-00167.1.

Sherwood, S., Webb, M. J., Annan, J. D., Armour, K. C., Forster, P. M., Hargreaves, J. C., et al. (2020). An assessment of Earth's climate sensitivity using multiple lines of evidence. *Reviews of Geophysics*, 58, e2019RG000678, doi: 10.1029/2019RG000678 .

Shine, K.P., and P.M.Forster, 1999: The effect of human activity on radiative forcing of climate change: a review of recent developments. *Glo. Plan. Ch.*, 20, 4, doi:10.1016/S0921-8181(99)00017-X.

Shine, K. P., Cook, J., Highwood, E. J., and Joshi, M. M., 2003: An alternative to radiative forcing for estimating the relative importance of climate change mechanisms, *Geophys. Res. Lett.*, 30, 2047, doi:10.1029/2003GL018141, 20.

Smith, C. J., Kramer, R. J., Myhre, G., et al., 2020: Effective radiative forcing and adjustments in CMIP6 models, Atmos. Chem. Phys., 20, 9591–9618, https://doi.org/10.5194/acp-20-9591-2020.

Smith, C. J., Kramer, R. J., and Sima, A., 2020: The HadGEM3-GA7.1 radiative kernel: the importance of a well-resolved stratosphere, Earth Syst. Sci. Data Discuss., In press, https://doi.org/10.5194/essd-2019-254.

Smith, C.J., R.J. Kramer, G. Myhre, P.M. Forster, B.J. Soden, T. Andrews, et al. 2018: Understanding rapid adjustments to diverse forcing agents. *Geophysical Research Letters*, 45, 12023-12031, doi:10.1029/2018GL079826.

Soden, B. J., I. M. Held, R. Colman, K. M. Shell, J. T. Kiehl, and C. A. Shields, 2008: Quantifying Climate Feedbacks Using Radiative Kernels. *J. Climate*, 21, 3504–3520, doi: 10.1175/2007JCLI2110.1.

Tang, T., et al., 2019: Comparison of Effective Radiative Forcing Calculations using Multiple Methods, Drivers, and Models. JGR, 124, 4382– 4394. doi: 10.1029/2018JD030188.

Taylor, K. E., R. J. Stouffer, and G. A. Meehl, 2012: An Overview of CMIP5 and the Experiment Design. Bull. Amer. Meteor. Soc., 93, 485–498, doi: 10.1175/BAMS-D-11-00094.1.

Wyant, M. C., Bretherton, C. S., Blossey, P. N., and Khairoutdinov, M. , 2012: Fast cloud adjustment to increasing CO_2 in a superparameterized climate model, *J. Adv. Model. Earth Syst.*, 4, M05001, doi:10.1029/2011MS000092.

Zarakas, C. M., A. L. S. Swann, M. M. Laguë, K. C. Armour, and J. T. Randerson, 2020: Plant Physiology Increases the Magnitude and Spread of the Transient Climate Response to CO_2 in CMIP6 Earth System Models. *J. Climate*, 33, 8561–8578, doi: 10.1175/JCLI-D-20-0078.1.

Zelinka, M. D., Myers, T. A., McCoy, D. T., Po-Chedley, S., Caldwell, P. M., Ceppi, P., et al., 2020: Causes of higher climate sensitivity in CMIP6 models. *Geophysical Research Letters*, 47, e2019GL085782m, doi: 10.1029/2019GL085782.

Zelinka, M. D., S. A. Klein, and D. L. Hartmann, 2012: Computing and Partitioning Cloud Feedbacks Using Cloud Property Histograms. Part I: Cloud Radiative Kernels. *J. Climate*, 25, 3715–3735,doi: 10.1175/JCLI-D-11-00248.1.

Zhou, C. , M. D. Zelinka, and S. A. Klein, 2016: Impact of decadal cloud variations on the Earth's energy budget. Nat. Geosci., 9, 871– 874, doi: 10.1038/ngeo2828.

Table 1: Global-mean Effective Radiative Forcing (ERF) and radiative adjustments in ACCESS1.0 4xCO_2, 4xCO_2-rad and +Solar fixed-SST and fixed-T_s (SST and land) ERF simulations. ERF is the change in net TOA radiative flux in the perturbation experiment relative to it's control. Adjustments are estimated via radiative kernel calculations (see Section 2.2). Also shown is the global-mean surface temperature change (ΔT_s) and surface-air-temperature change (ΔT) in each experiment. We interpret the difference (fixed-SST minus fixed-T_s) as the radiative effect of land warming and associated radiative adjustments (termed the 'land effect' here). In 4xCO_2-rad the CO_2 is quadrupled only in the radiation scheme. Hence the comparison of 4xCO_2 to 4xCO_2-rad quantifies the CO_2 stomatal effect. +Solar forcing represents an increase in the solar constant by ~3.3%.

Forcing	Experimental Design	ERF (Wm^{-2})	Sum of Radiative Adjustments (Wm^{-2})	Adjustments (Wm^{-2})							ΔT_s (K)	ΔT (K)
				$Planck_{surf}$ ($A_{Planck_{surf}}$)	$Planck_{trop}$ ($A_{Planck_{trop}}$)	Lapse-rate (A_{LR})	Water Vapour (A_q)	Strat T (A_{strat})	Surface Albedo (A_α)	Cloud (A_c)		
4xCO_2	Fixed-SST	7.03	1.46	-0.48	-1.15	0.01	0.32	2.07	0.15	0.54	0.51	0.56
	Fixed-T_s	7.98	2.42	-0.03	-0.06	-0.18	-0.17	2.08	-0.02	0.80	0.04	0.13
	Land Effect	-0.95	-0.96	-0.45	-1.09	0.19	0.49	-0.01	0.17	-0.26	0.47	0.43
4xCO_2-rad	Fixed-SST	6.79	1.20	-0.35	-0.72	-0.39	0.39	2.04	0.15	0.08	0.34	0.40
	Fixed-T_s	7.19	1.64	-0.04	-0.07	-0.64	0.18	2.07	0.02	0.12	0.04	0.13
	Land Effect	-0.40	-0.44	-0.31	-0.65	0.25	0.21	-0.03	0.13	-0.04	0.30	0.27
+Solar	Fixed-SST	7.13	-0.97	-0.26	-0.54	-0.42	0.61	-0.31	0.13	-0.18	0.24	0.25
	Fixed-T_s	7.52	-0.56	-0.01	-0.01	-0.51	0.38	-0.29	0.02	-0.14	0.01	0.05
	Land Effect	-0.39	-0.41	-0.25	-0.53	0.09	0.23	-0.02	0.11	-0.04	0.23	0.20

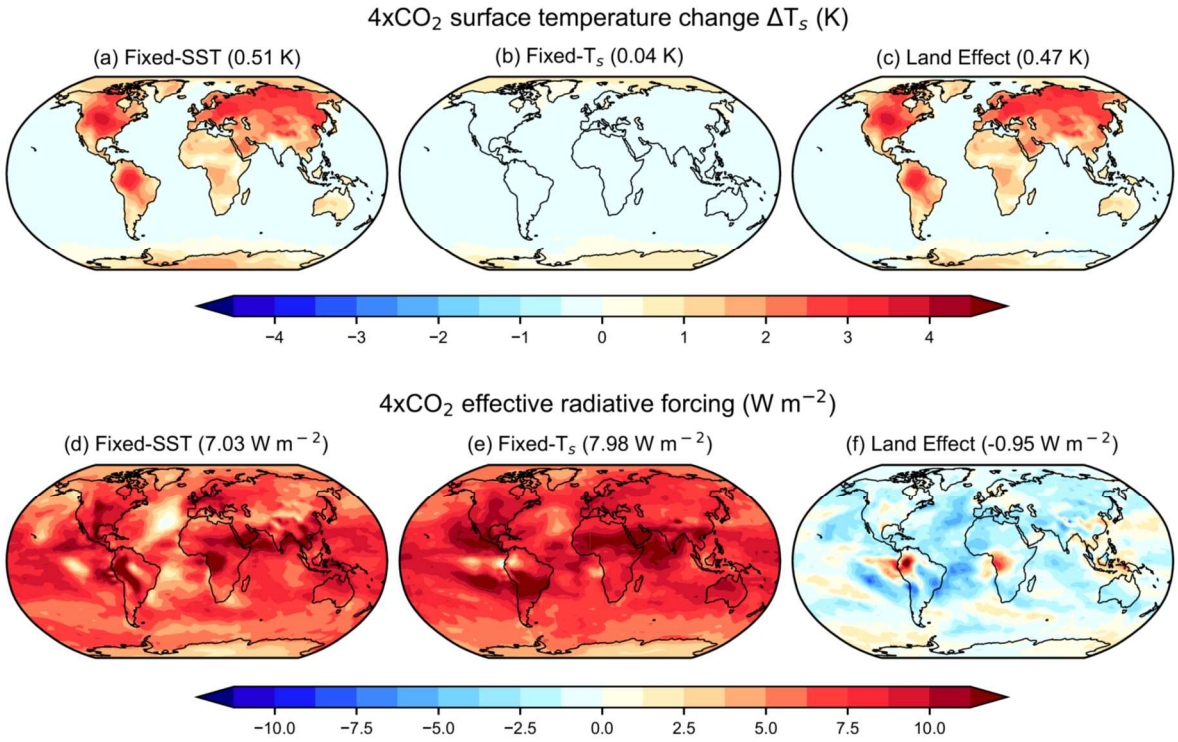

Figure 1: Change in surface temperature, ΔT_s, in the 4xCO_2 (a) fixed-SST and (b) fixed-T_s experimental designs. The difference, which we interpret as the land surface warming in the fixed-SST experiment, is shown in (c). (d) and (e) show the 4xCO_2 effective radiative forcing (ERF) in the fixed-SST and fixed- T_s experimental designs respectively. The difference, which we interpret as the radiative effect of land surface warming and associated adjustments in the fixed-SST experiment, is shown in (f).

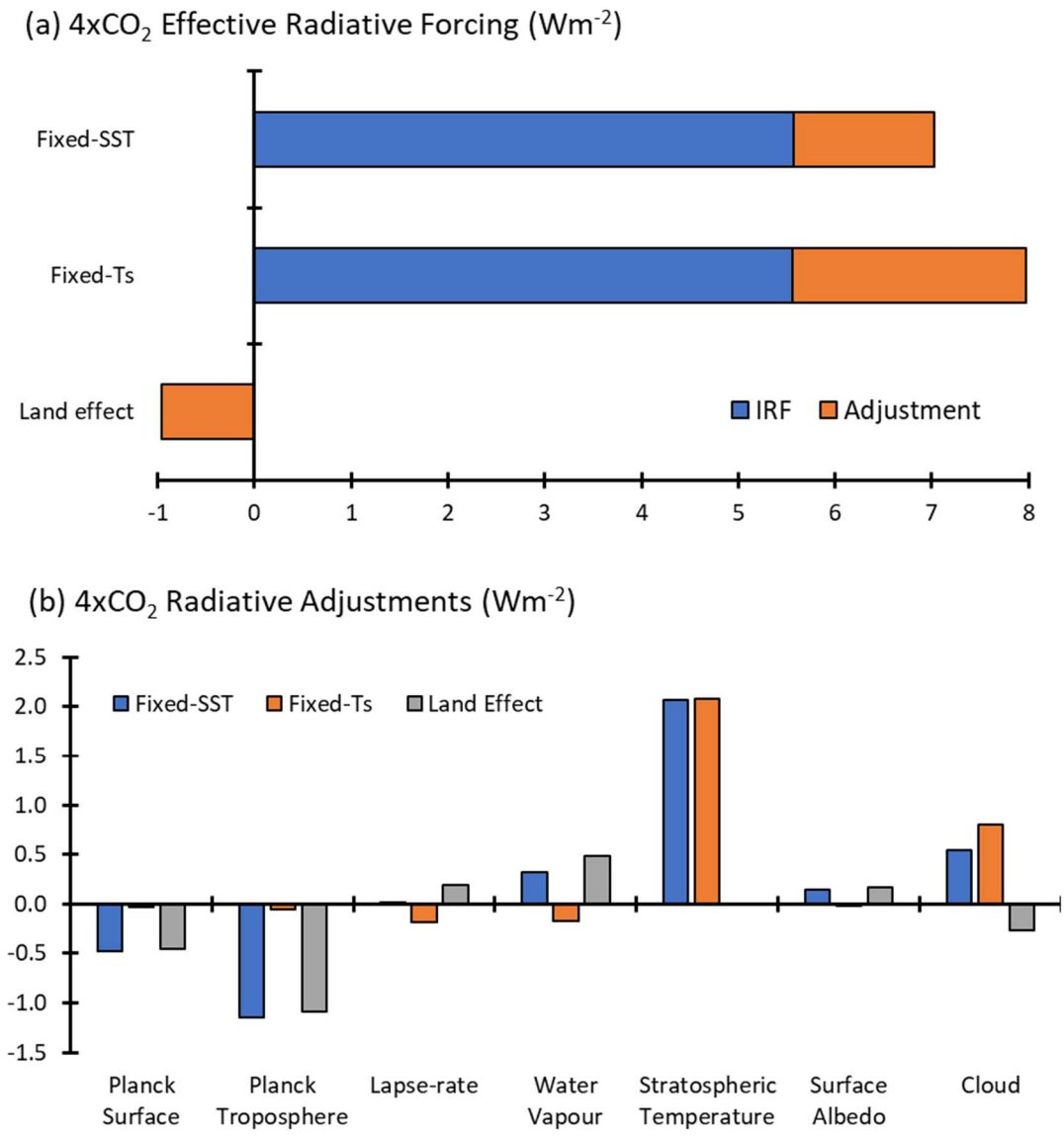

Figure 2: (a) Global-mean 4xCO_2 ERF and its separation into Instantaneous Radiative Forcing (IRF) and radiative adjustments in the fixed-SST and fixed-T_s experimental designs. IRF is simply the difference between the ERF and sum of the adjustments in Table 1. The land effect is the difference between the fixed-SST and fixed-T_s results. (b) Comparison of the global-mean 4xCO_2 radiative adjustments (see Section 2.2 and Table 1) in the different ERF experimental designs.

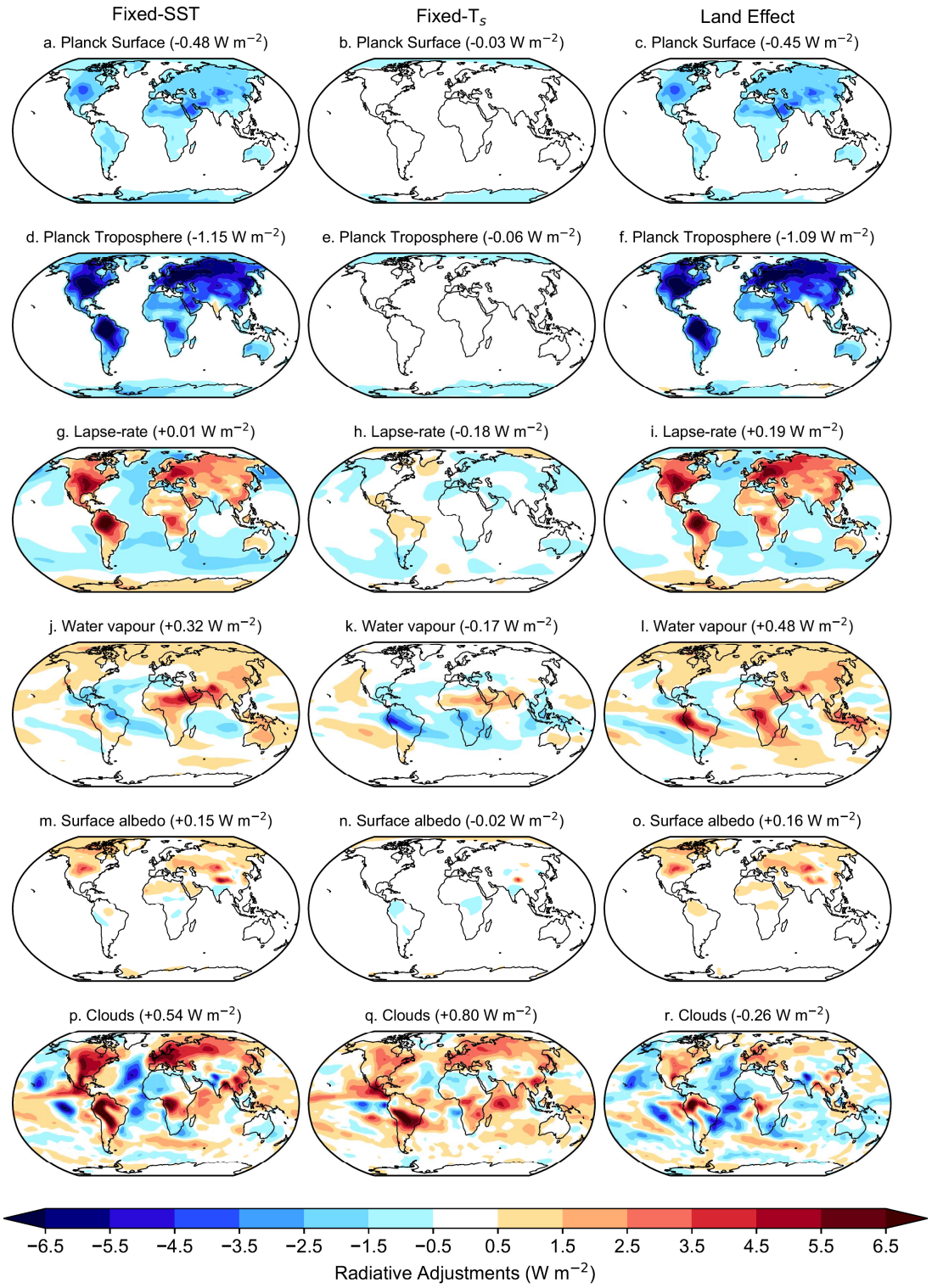

Figure 3: 4xCO_2 radiative adjustments in the fixed-SST (left column) and fixed-T_s (middle column) experimental designs. (Right column) Radiative adjustments associated with the land surface temperature change in the 4xCO_2 fixed-SST experiment, calculated as the difference in adjustments in the fixed-SST and fixed-T_s designs.

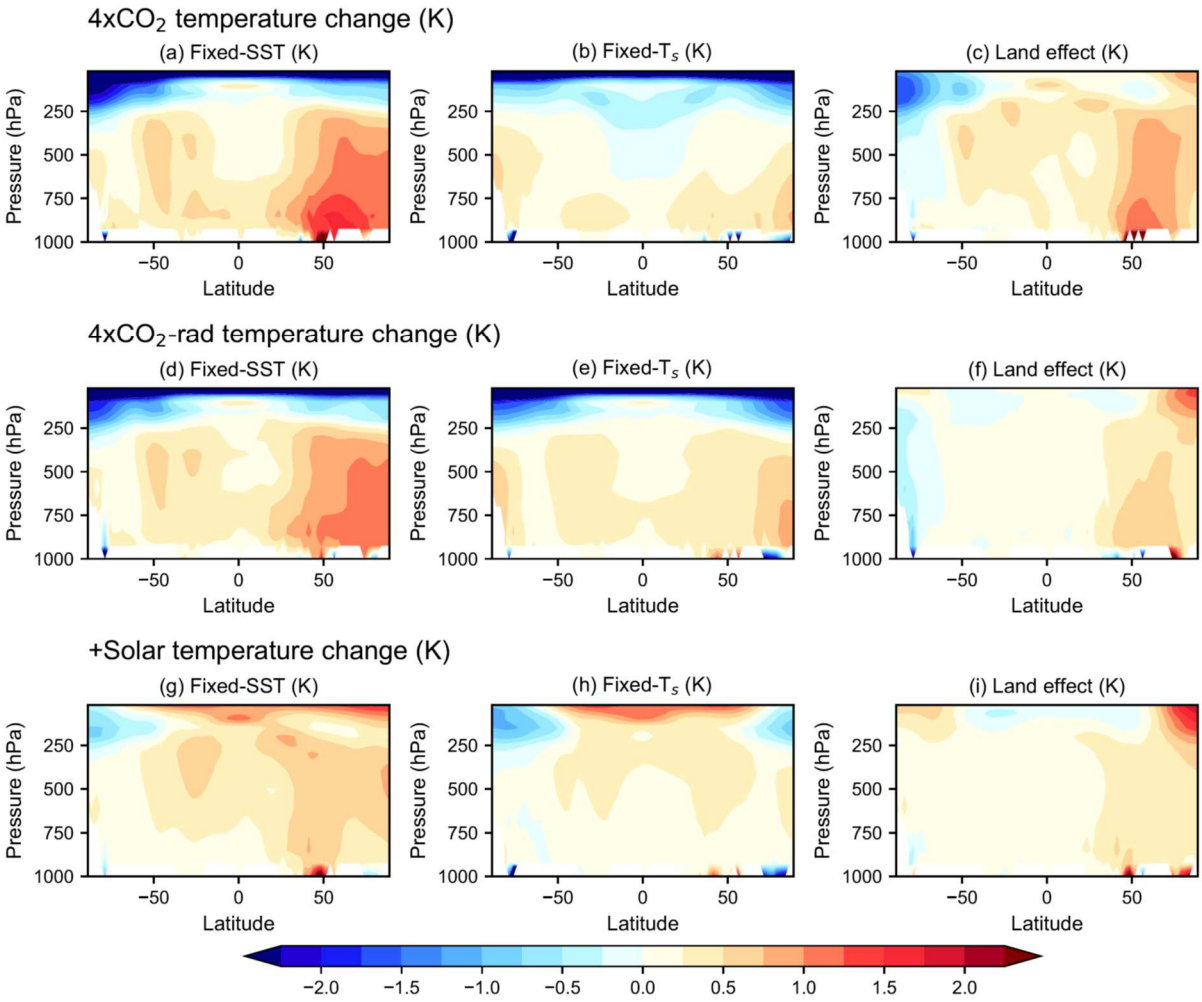

Figure 4: Change in zonal-mean temperature, in the (a-c) 4xCO_2 experiments, (d-f) 4xCO_2-rad experiments, and (g-i) +Solar experiments. (Left column) fixed-SST, (middle column) fixed-T_s and (right column) their difference (i.e. the land surface warming effect).

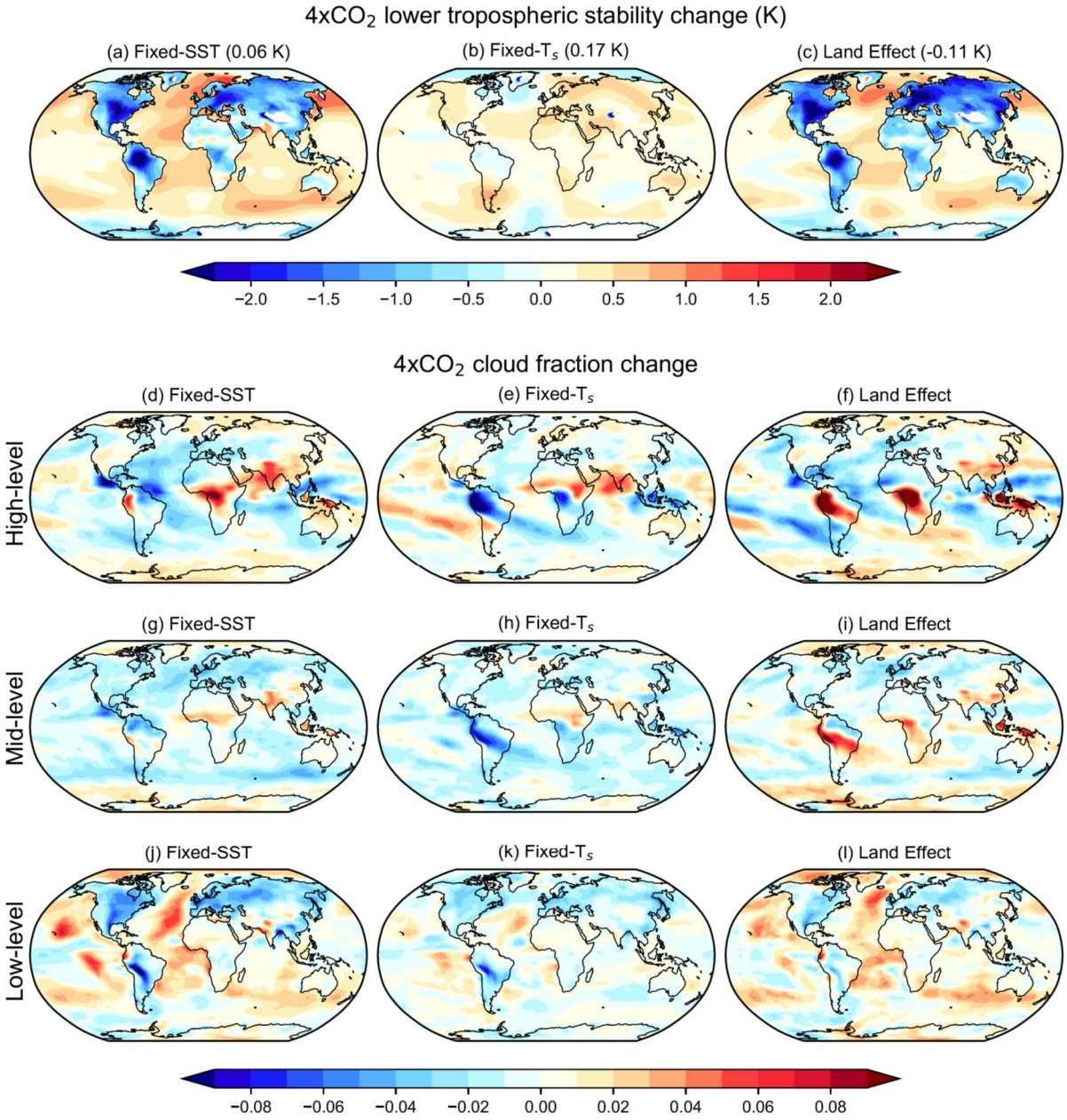

Figure 5: Change in lower tropospheric stability, defined simply as the difference in air temperature at 700mb and the surface, in the (a) fixed-SST and (b) fixed-T_s 4xCO_2 experimental designs, and their difference (c) the land effect. Change in (d-f) high-level cloud fraction (see text), (g-i) mid-level cloud fraction (see text), and (j-l) low-level cloud fraction (see text), in the (left column) fixed-SST, (middle column) fixed-T_s 4xCO_2 ERF experimental designs, and their difference (right column) the land effect.

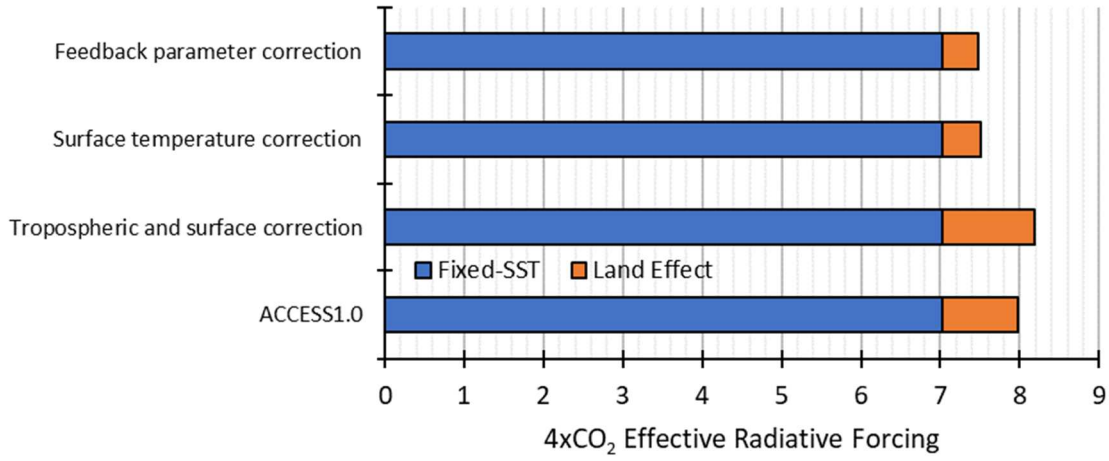

Figure 6: Comparison of the various methods proposed to correct fixed-SST ERF estimates for land surface temperature change against our ACCESS1.0 GCM results. In each case, the blue bar is the $4xCO_2$ fixed-SST ERF as simulated by ACCESS1.0 to which a land warming effect (orange) is added (as determined by the various methods described below and in Section 4) to give a corrected $4xCO_2$ ERF (total bar). The bottom row shows the actual land warming effect as simulated by the GCM (the total bar being the fixed-T_s ERF). The 'feedback parameter correction' method scales the global-mean surface-air-temperature change in the fixed-SST simulation by the model's known feedback parameter (Section 4.1). The 'surface temperature correction' method accounts directly for the land surface temperature change in the fixed-SST simulation by calculating its radiative effect via radiative kernels (see Section 4.2). The 'tropospheric and surface correction' method extends the surface temperature correction to include other adjustments from the fixed-SST experiment that can reasonably be assumed to be associated with the land surface temperature change, such as changes in surface albedo and a component of tropospheric temperature and water-vapour change (see Section 4.3).